

Weakly-supervised Micro- and Macro-expression Spotting Based on Multi-level Consistency

Wang-Wang Yu, Kai-Fu Yang, Hong-Mei Yan, and Yong-Jie Li, *Senior Member, IEEE*

Abstract—Most micro- and macro-expression spotting methods in untrimmed videos suffer from the burden of video-wise collection and frame-wise annotation. Weakly-supervised expression spotting (WES) based on video-level labels can potentially mitigate the complexity of frame-level annotation while achieving fine-grained frame-level spotting. However, we argue that existing weakly-supervised methods are based on multiple instance learning (MIL) involving inter-modality, inter-sample, and inter-task gaps. The inter-sample gap is primarily from the sample distribution and duration. Therefore, we propose a novel and simple WES framework, MC-WES, using multi-consistency collaborative mechanisms that include modal-level saliency, video-level distribution, label-level duration and segment-level feature consistency strategies to implement fine frame-level spotting with only video-level labels to alleviate the above gaps and merge prior knowledge. The modal-level saliency consistency strategy focuses on capturing key correlations between raw images and optical flow. The video-level distribution consistency strategy utilizes the difference of sparsity in temporal distribution. The label-level duration consistency strategy exploits the difference in the duration of facial muscles. The segment-level feature consistency strategy emphasizes that features under the same labels maintain similarity. Experimental results on two challenging datasets—CAS(ME)² and SAMM-LV—demonstrate that MC-WES is comparable to state-of-the-art fully-supervised methods.

Index Terms—Micro- and macro-expression spotting, weakly-supervised learning, multi-level consistency, multiple instance learning

1 INTRODUCTION

Facial expression is an important medium for conveying human emotions. Expressions can be categorized as micro-expressions (MEs) and macro-expressions (MaEs) [1]. MEs are subtle, involuntary facial movements and often occur when a person tries to conceal or suppress his or her true emotion. MEs contain three prominent features on the face—short duration, low intensity, and local movement [2]—making them difficult even for experienced experts to recognize [3]. In contrast, MaEs are visible facial motion processes with distinct start and end temporal points and variable durations. Compared with MaEs, which may convey inauthentic emotions, MEs reflect real changes in emotion, and are therefore useful in high-stakes environments such as medical diagnosis, public safety, crime investigation and political business negotiation [4], [5].

Expression analysis includes the major tasks of spotting and recognition. Recognition aims to identify facial expressions as belonging to specific emotional categories [6] or continuous multidimensional values [7], [8], [9]. Spotting, as a prior task, focuses on localizing key continuous intervals from an untrimmed long video and classifying them as MEs and MaEs. As it is difficult to quantify the intensity and range of the movement of expressions, the duration of MaEs and MEs is naturally seen as a benchmark for classification

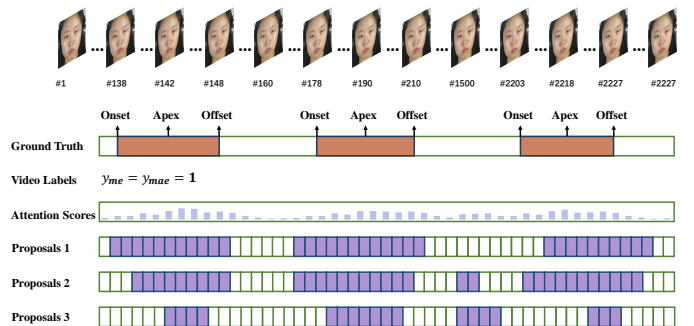


Fig. 1. A video of S15_0502 with the range of frames #1 to #2273 from the CAS(ME)² dataset. There are three ground truth intervals, which are from #138 to #148, #178 to #210, and #2203 to #2227. The first interval contains a micro-expression, and the last two contain macro-expressions. Frames #138, #178 and #2203 are the onset frames, frames #142, #190 and #2218 are the apex frames, and frames #148, #210 and #2227 are the offset frames. Therefore, video-level labels of this video contain both micro-expression and macro-expression classes, i.e., $y_{me} = y_{mae} = 1$. In the pre-processing phase, the video is divided into a series of uniform non-overlapping snippets. During training, we generate attention scores indicating actionness scores (probabilities belonging to foreground) with the video-level labels. During testing, these attention scores are used to generate multiple proposals with different top- k values. The goal is to spot several consecutive video snippets as close as possible to ground truth intervals.

- W. Yu, K. Yang, H. Yan and Y. Li are with MOE Key Lab for Neuroinformation, University Of Electronic Science And Technology Of China, Chengdu, China. Email: yuwangwang91@163.com, yangkf@uestc.edu.cn, hmyan@uestc.edu.cn, lij@uestc.edu.cn

Manuscript received April 19, 2005; revised August 26, 2015. (Corresponding author: Yong-Jie Li.)

on all main spotting datasets, including CAS(ME)² [10], SAMM-LV [11], MMEW [12], and CAS(ME)³ [13], based on the statistical fact that MaEs last from 0.5 to 4.0 seconds, while MEs occur in less than 0.5 second [4]. To portray the whole change of facial movements with a more fine-grained

description, an expression can be described by three key temporal points—onset, apex, and offset [2]—as illustrated in Figure 1. The onset is the starting time, the apex demonstrates the most noticeable emotional information under maximum facial muscle deformation [14], [15], and the offset is the ending time. From this perspective, datasets for the spotting task furnish the onset, offset, and apex frames of all ground truths for model learning.

ME and MaE spotting have been shown to be successful in long untrimmed videos based on frame-by-frame annotations in a fully-supervised setting [16], [17]. However, extensive video-level acquisition relies heavily on carefully designed experimental environments and stimulus conditions [10], [11], [12], [13]. Moreover, obtaining fine-grained frame-level labels requires extensive manual labor involving two or more coders, with an average of two hours required to annotate one minute of ME and MaE videos [18]. These bring difficulty in rolling out ME-related applications on a large scale.

There is a growing availability of diverse face videos with emotion labels on the internet, providing a potential source for data collection. Although such video-level labels are essentially weak labels, they provide direct emotional clues. This motivates us to develop an effective weak label-based ME and MaE spotting method. Our goal is to achieve automatic weakly-supervised expression spotting (WES) with only video-level (weak) labels, as illustrated in Figure 1. Obtaining these video-level labels, however, presents a challenge. Most spotting datasets [10], [12], [13] rely on labeling action units (AUs) to determine the onset and offset frames of ground truth intervals. Then coders classify the labeled intervals into MEs and MaEs based on their durations. Therefore, a simple method of weakly-supervised video annotation is to still use the annotation method adopted for the above datasets, and once the coders find one ME and one MaE in a video, it is considered annotated. This can significantly reduce the time and manual effort required for annotation.

WES is based on multiple instance learning (MIL) [19], which implies the need to construct a package of positive and negative samples. To this end, we divide the video into uniform non-overlapping snippets¹ as instances. The essence of WES task is that, during training, only the expression categories (ME, MaE) contained in the video are given, but not the number of expressions and the onset and offset frames. During testing, this task localizes and classifies intervals by calculating the differences in the snippets and aggregating continuous snippets to generate proposals.

To date, several MIL-based methods [21], [22], [23] have been proposed for the weakly-supervised temporal action localization (WTAL) task. However, when we try to apply the MIL-based method directly to the WES framework, inter-model, inter-sample and inter-task gaps are produced. The inter-modal gap occurs due to the use of features from two modalities, raw images and optical flow, as input in two-stream networks [21], [22], [23], [24]. Although optical flow can provide enough motion information and raw images can provide enough appearance information [25], [26],

the features from the two modalities are inconsistent [27]. The inter-sample gaps are primarily manifested in sample distribution and duration. Specifically, the distribution reflecting the frequency of sample appearance is not uniform because MEs are more dependent on harsh excitation conditions than MaEs [10], [11], while the duration varies for different actions due to the definitions of the two types of expressions in terms of duration [28]. The inter-task gap refers to the discrepancy between the localization and classification tasks [29], [30], [31]. Models supervised with video-level information only, tend to favor the most discriminative snippets or the contextual background, which contribute most to video-level classification [32].

To mitigate the above multiple gaps and merge more prior knowledge in weakly-supervised frameworks, we propose a framework, MC-WES, which employs the collaboration of multi-level consistency to spot more fine-grained expression intervals with video-level labels. The WC-WES framework includes four consistency strategies: (i) modal-level saliency consistency; (ii) video-level distribution consistency; (iii) label-level duration consistency; (iv) segment-level feature consistency. Considering that the differences between appearance (raw images) and movement (optical flow) modalities may lead to the incorporation of redundant information [21], the suboptimal models using direct fusion [33], [34], and the discarding of salient features of inter-modal asynchronization [27], we use a modal-level saliency consistency strategy to design a core saliency compensation module (CSCM), aiming to capture key correlations between the two modalities and alleviate suboptimality from different modalities, while integrating the strengths of each.

Due to the strict stimulus conditions and the short duration of MEs, their distribution is significantly sparser than that of MaEs, while maintaining the same snippet duration [10], [11]. To merge prior knowledge about the distribution, our video-level distribution consistency strategy generates the average logits (i.e., values representing the category responses before processing by the softmax function) in the MIL-based pipeline by using different top- K values² for different classes corresponding to their temporal sparsities, which is unlike the traditional use of the same value in the top- K to sample the logits of each category [21], [35], [36].

The duration of MEs is shorter than that of MaEs [2], [4]. When the duration of an ME is restricted to no more than a specified number of snippets, our label-level duration consistency strategy calculates the deviation in mean attention scores of neighboring snippets to remove potential ME intervals. The remaining snippets are then likely to be MaEs and backgrounds.

To highlight the similarity of features within the same categories, previous works [21], [23] use a co-activity similarity loss to generate the element-wise probabilities of video logits, and then embeds probabilities into video features to minimize intra-class differences and maximize inter-class differences. However, when the dimension of a video feature is 2048 and the logits from a classifier are activated by a softmax function along the temporal dimension, aggregation results can be overly smoothed by the co-activity sim-

1. In this paper, we treat snippets as the smallest granularity, and intervals as sequences consisting of one or more consecutive snippets.

2. In this paper, the top- k contains a parameter to be specified, while top- K contains k_1, \dots, k_n where the i -th class corresponds to the parameter of k_i .

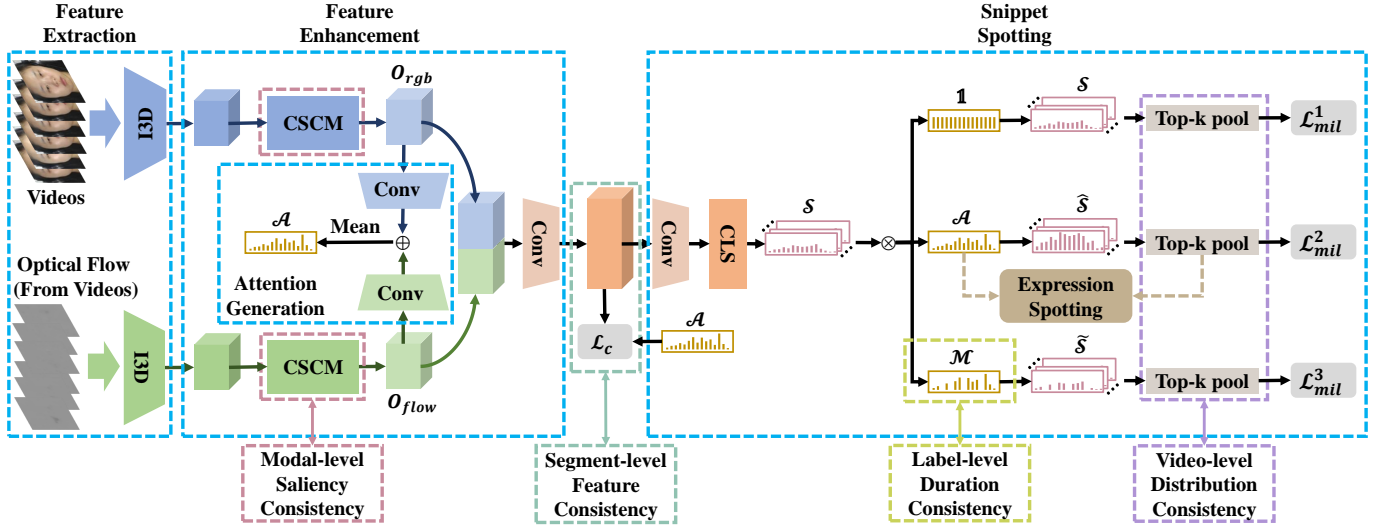


Fig. 2. Overall schematic of proposed MC-WES. Given a video, snippet-level features are extracted by the two-stream Inflated 3D ConvNets (I3D) model [20] from a set of uniform non-overlapping snippets sampled from videos and optical flow. CSCM is the core saliency compensation module used to fuse core features and filter irrelevant features for each modality. Processed features (i.e., O_{rgb} and O_{flow}) are used to generate attention scores. Mean attention scores \mathcal{A} of two modalities represent probability that snippets belong to the foreground. These processed features are also concatenated and fed into a convolution layer to produce modal-enhanced features used to implement the segment-level feature consistency strategy to optimize features corresponding to top- k attention scores and calculate attention-guided feature consistency loss \mathcal{L}_c . Modal-enhanced features are subsequently fed into classifier CLS to generate temporal class activation maps (T-CAMs) \mathcal{S} , which indicate logits for each category of video. T-CAMs \mathcal{S} are used to fuse with all-1 matrix $\mathbf{1}$, attention scores \mathcal{A} , and strategy-filtered mask matrix \mathcal{M} , respectively. Three branches of fused T-CAMs \mathcal{S} are processed with the video-level distribution consistency strategy, where we utilize temporal top- K pooling layers to aggregate logits and calculate MIL-based losses (i.e., $\mathcal{L}_{mil}^1, \mathcal{L}_{mil}^2, \mathcal{L}_{mil}^3$). Note that we calculate the variation to generate the mask matrix \mathcal{M} in attention scores between snippets within a certain range, and then implement the label-level duration consistency strategy based on MIL to highlight difference in duration between MEs and MaEs. During testing, we utilize T-CAMs $\hat{\mathcal{S}}$ and mean attention scores \mathcal{A} to generate expression proposals.

ilarity loss. Therefore, we utilize temporal attention scores to localize potential ME and MaE snippets [21], [23], and integrate snippet-level features and background-foreground temporal attention scores to build the segment-level feature consistency strategy. Specifically, we calculate the similarity between the video features corresponding to the top- k attention scores and those of the other one in the video pair, whose labels are at least partially consistent. The maximum snippet-level feature similarities along selected attention score dimension corresponding to the video should be as consistent as possible with the attention scores of the other video.

We summarize our main contributions as follows:

- To the best of our knowledge, this is the first work to utilize a weakly-supervised MIL-based learning framework for ME and MaE spotting in untrimmed face videos with only coarse video-level labels and no fine-grained frame-level annotations.
- We propose a modal-level saliency consistency strategy based on CSCM to address information redundancy and alleviate inter-modal asynchronization between raw images and optical flow.
- To merge the prior knowledge about the sample distribution and duration between MEs and MaEs, we present a video-level distribution consistency strategy and a label-level duration consistency strategy.
- A segment-level feature consistency strategy is proposed to highlight the similarity of features within the same categories.
- Extensive experiments on the commonly used CAS(ME)² and SAMM-LV datasets demonstrate that

the effectiveness of our weakly-supervised MC-WES framework is comparable to that of fully-supervised expression spotting models.

2 RELATED WORK

2.1 Fully-supervised Expression Spotting

According to the type of the generated proposals, fully-supervised spotting methods based on deep learning can be classified as either key frame- or interval-based. Key frame-based methods [37], [38], [39], [40] aim to localize expression intervals by looking through one or more frames in a long video. Pan et al. [37] identify each frame as MaE, ME, or background frame, which results in the loss of positive samples. In contrast, SMEConvNet [38] uses one frame to spot intervals. However, most proposals generated by SMEConvNet tend to be of short duration. Yap et al. [39] rely on a few fixed durations, which may generate a large number of negative samples. SOFTNet [40] uses a shallow optical flow three-stream convolutional neural network (CNN) to predict whether each frame belongs to an expression, and introduces pseudo-labeling to facilitate the learning process.

Interval-based approaches [2], [17], [41], [42], [43] take all the image features in the video as input, and pay attention to the information of neighboring frames. To this end, long short-term memory (LSTM) is commonly used to encode neighbor temporal information [41], [42], [43]. However, LSTM cannot handle longer and more detailed temporal information. Wang et al. [2] utilize a clip proposal network to initially build long-range temporal dependencies by

combining different scales and types of convolution layers with downsampled features. LSSNet [17] uses anchor-based and anchor-free branches to generate multi-scale proposal intervals based on snippet-level features from raw images and optical flow.

Fully-supervised expression spotting methods can generally achieve relatively good performance, but they rely heavily on frame-level annotation which greatly increases the cost of data labeling and discourages the implementation of expression-related applications. In contrast, weakly-supervised spotting methods only use the relatively effort-less video-level labels to achieve frame-level localization.

2.2 Weakly-supervised Temporal Action Localization

Utilizing weak labels to train models has come a long way in computer vision such as semantic segmentation [44], [45], [46], object detection [47], [48], and temporal action localization (TAL) [21], [22], [23]. In contrast to the fully-supervised TAL [49], [50], [51], [52], the WTAL methods are free of extensive frame-level annotations and adopt video-level [23], [53], [54], [55], [56] or point (key frame)-level [57], [58], [59], [60] labels during training. Since different video-level WTAL approaches have different emphases, we can categorize them as foreground-only, background-assisted or pseudo-label-guided.

Foreground-only WTAL methods focus on extracting effective foreground information. UntrimmedNet [53] introduces MIL, where treats snippets as separate instances, which are also used in selection and aggregation to obtain proposals. Later, STPN [54] adds temporal class activation maps (T-CAMs) to generate one-dimensional temporal attentions, and aggregates proposals by adaptive temporal pooling operation. W-TALC [23] utilizes a co-activity similarity loss in the video pairs to enhance the similarity of identically labeled snippets and the variability of differently labeled snippets. To integrate multi-scale temporal information, CPMN [56] uses a cascaded pyramid mining network. 3C-Net [61] employs center and counting losses to learn more discriminative action features.

Foreground-only WTAL methods do not take background frames as a separately guided class during training, although there are contexts in them associated with actions. DGAM [63] divides a “longjump” action into approaching, jumping and landing stages, in which preparing and finishing are the most crucial contexts. To complete the modeling of the entire action, background-assisted methods generally build multi-branch or multi-stage architectures. CMCS [29] uses a diversity loss to model integral actions, and a hard negative generation module to separate contexts. BaSNet [35] adopts an attention branch to suppress background interference. DGAM [63] utilizes a two-stage conditional variational auto-encoder (VAE) [64] to separate action and context frames. HAM-Net [22] models an action as a whole based on multiple temporal attention scores consisting of soft, semi-soft and hard attention.

To minimize the discrepancy between classification and localization, many current methods generate pseudo labels during training. RefineLoc [65] iteratively generates pseudo ground truths that are used as supervised information to refine predictions for the next iteration. EM-MIL [66] uses

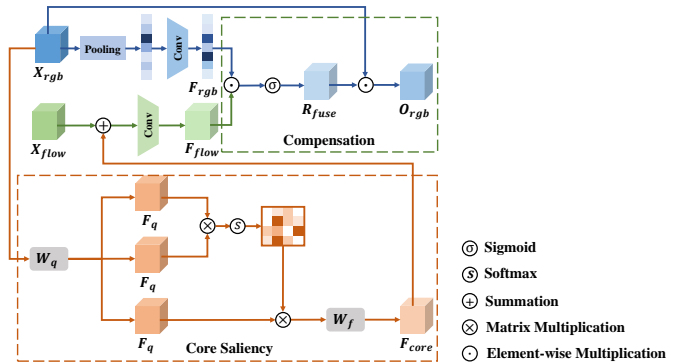


Fig. 3. Core Saliency Compensation Module (GSCM). We utilize the raw image or optical flow modality as the main branch and the other as the supporting branch. The main branch is used to extract core saliency (long-range element-wise dependency) information F_{core} and element-wise squeezer F_{rgb} . Core saliency unit is part of self-attention mechanisms [62], with only one 1×1 convolution layer W_q . Output F_{core} from core saliency unit complements significant information and reinforces the modal coherence information between two modalities in the supporting branch. The enhanced supporting branch cooperates with element-wise squeezer F_{rgb} to generate compensation unit R_{fuse} , which is modulated by a sigmoid function. Features from the main branch are enhanced by modulated R_{fuse} as final output O_{rgb} .

an expectation maximization algorithm to improve pseudo-label generation. ASM-Loc [24] introduces a re-weighting module for pseudo label noise effects with an uncertainty prediction module [55]. EM-Att [32] mines the discriminative snippets and propagates information between snippets to generate pseudo labels.

Compared with video-level WTAL methods, point-level WTAL methods add a small amount of supervised information to determine more accurate action boundaries. Moltisanti et al. [67] introduce the point-level labels, and further alleviate the gap between the continuously increasing number of different actions and weak video-level labels. SF-Net [60] adopts a pseudo label mining strategy to acquire more labeled frames for the point-level WTAL task. LACP [57] takes the points to search for optimal sequences, which are used to learn completeness of entire actions. Ju et al. [59] divide entire video into multiple video clips, and use a two-stage network to localize the action instances in each one.

We choose the video-level framework, even though point-level methods have been shown to produce better results, primarily because the intensity and duration of the expressions are weaker and shorter than those of the general actions in WTAL, which makes point-level annotation of expressions much more costly.

2.3 Multiple Instance Learning

In a weakly-supervised learning framework based on coarse-grained labeling, MIL [19] has been proven to be the most effective solution, whose essence is to build a positive bag, where at least one sample is positive, and a negative bag, in which all samples are negative. Several tasks, including semantic segmentation and object detection, utilize region proposal techniques to generate these bags [44], [45], [46], [47], [48]. In WTAL, most methods sample a large number of snippets from each video to construct the bags [21], [22], [23].

Because currently published action localization datasets [68], [69] commonly have more than 20 action categories, MIL-based methods [21], [22], [23] do not focus on the differences between categories. In contrast, the spotting task in this paper involves only the categories of MEs and MaEs, allowing us to integrate their differences for more precise localization. We work on distribution and duration without focusing on the intensity and range of face movements in our MC-WES framework. To achieve this, we incorporate duration information into the attention scores to process logits using multiple branches, and aggregate processed multiple logits using the different values in the top- K based on distribution information to construct our MIL-based method.

3 METHODOLOGY

We present a novel and simple weakly-supervised ME and MaE spotting framework, MC-WES, with only video-level weak labels to complete frame-level expression spotting.

3.1 Problem Formulation

Assume a video $V = \{v_t\}_{t=1}^L$ has L frames and contains n expression categories with video-wise labels $y_c \in \{1, 0\}^{n+1}$, where $n + 1$ is the number of expression categories that contain the background class. $y_i = 1$ means that there is at least one instance of the i -th expression, and if $y_i = 0$, there is no such instance. In WES framework, the number and the order of expressions in the video are not provided in the training phase. During testing, expression proposals $E = (f_{on}, f_{off}, y, \phi)$ are generated, where f_{on} denotes the onset frame, f_{off} denotes the offset frame, y denotes the category, and ϕ indicates the confidence score. Note that f_{on} and f_{off} are integer multiples of the number of frames in the snippets, because we only localize specific snippets to generate proposal intervals. Following a previous approach [17], we only need to filter the samples with confidence scores and then calculate the recall and precision based on the duration of the proposals, defining those below 0.5 second as MEs and those longer than that as MaEs instead of the classification results of the model.

3.2 Framework Overview

As shown in Figure 2, our MC-WES framework has four components: feature extraction, feature enhancement, attention generation, and snippet spotting.

Feature Extraction. We first generate optical flow from a video and then divide the video and optical flow into a series of uniform non-overlapping snippets, each containing g frames. We use the two-stream Inflated 3D ConvNets (I3D) model [20] to extract image features $X_{rgb} \in \mathbb{R}^{T \times D}$ and optical flow features $X_{flow} \in \mathbb{R}^{T \times D}$ from these snippets, where $T = L/g$ is the number of snippets (to facilitate training, each video of the same dataset is sampled as the same number of snippets T), and D is the dimension of one snippet feature. To maintain the consistency of the numbers of raw images and optical flow, we delete the last frame of a video. The TV-L1 optical flow algorithm [70] with the default smoothing parameter ($\lambda = 0.15$) is used to generate a dense optical flow.

Feature Enhancement. To incorporate movement and appearance information, we take the features from the raw image and optical flow modalities as input following previous frameworks [21], [22], [35]. However, our input features are extracted from the I3D model used for action recognition, leading to feature redundancy [21]. In addition, the features are not synchronized due to the difference in modalities [27]. To address these issues, we employ a modal-level saliency consistency strategy to enhance features, which also enables feature synchronization and effective fusion between modalities simultaneously.

Attention Generation. Attention scores represent the probability that each snippet belongs to the foreground intervals in our MC-WES framework. We compute modal-specific temporal attention scores based on the enhanced modal-specific features as $\mathcal{A}_{rgb} \in \mathbb{R}^T$ for image modality and $\mathcal{A}_{flow} \in \mathbb{R}^T$ for optical flow modality [21]. Then we calculate the mean class-agnostic attention scores $\mathcal{A} = \frac{1}{2}(\mathcal{A}_{rgb} + \mathcal{A}_{flow})$ as guidance to process the class-specific logits of T-CAMs, which are generated by the following classifier. These mean attention scores are also used to select class-agnostic expression proposals during testing.

Snippet Spotting. Snippet spotting is used to optimize class-specific T-CAMs $\mathcal{S} \in \mathbb{R}^{T \times (n+1)}$, which indicate the logits of each snippet belonging to all categories [71]. Here, the $(n + 1)$ -th class is the background class. As shown in Figure 2, three branches process the logits of T-CAMs, two of which are coupled with the localization information derived from temporal attention scores.

3.3 Multi-level Consistency Analysis

Expression spotting is the temporal localization and binary classification task in untrimmed face videos, and is essentially an application of TAL in expression analysis. Due to the success of WTAL in video understanding, we apply it to expression analysis and introduce a WES framework. To fuse more prior information and alleviate existing gaps, including inter-modal, inter-sample and inter-task, we employ a multi-consistency collaborative mechanisms, with four consistency strategies: modal-level saliency, video-level distribution, label-level duration and segment-level feature consistency. In particular, the modal-level saliency consistency strategy is applied in feature enhancement to mitigate inter-modal gaps. The video-level distribution and label-level duration consistency strategies are used in snippet spotting to alleviate inter-sample gaps that arise from differences in distribution and duration. The segment-level feature consistency strategy is utilized for fused features to mitigate inter-task gaps, which are intermediate between the components of feature enhancement and snippet spotting.

Modal-level Saliency Consistency Strategy. Following previous frameworks [21], [22], [23], [35], [61], we perform our MC-WES framework using a two-stream network, and extract features from the original images and optical flow as input using the I3D model [20]. However, the I3D model is originally trained for video action recognition, and its extracted features always contain noisy information, which can degrade performance and lead to suboptimal training [72], [73]. CO₂-Net [21] adopts cross-modal consensus modules to reduce task-irrelevant information redundancy. The

process is a squeeze-and-excitation block from SENet [74]. However, the distributions of features from raw image and optical flow are temporally inconsistent [27]. As a result, the channel-wise descriptors generated by the cross-modal consensus module tend to weaken modal-inconsistent information and strengthen some modal-consistent irrelevant information. Inspired by these works, we design CSCM to extract task-specific features based on complementary enhanced features by encouraging the complementarity of global and core information between raw image and optical flow modalities.

To alleviate the information discrepancy caused by modality inconsistency, we use CSCM to extract the global core salient information of the main modality (i.e., raw images), which is used to enhance the auxiliary modality (i.e., optical flow). Then the enhanced auxiliary modality is integrated with the pooled elements of the main modality. Suppose the input features of raw images and optical flow are $X_{rgb} \in \mathbb{R}^{T \times D}$ and $X_{flow} \in \mathbb{R}^{T \times D}$, respectively, as shown in Figure 3. The input features of raw images are squeezed by an adaptive average pooling layer as a modal-specific global vector, which is used to aggregate information,

$$F_{rgb} = \sigma(W_{rgb} \cdot (\frac{\sum_{t=1}^T (X_{rgb})}{T}) + B_{rgb}), \quad (1)$$

where W_{rgb} is a 3×3 convolution layer, $B_{rgb} \in \mathbb{R}^D$ is the bias of convolution layer W^{rgb} , and σ is a sigmoid function to ensure the generated weights are between 0 and 1. We also take simple self-attention mechanisms [62] with only one 1×1 convolution layer and without a shortcut operation to process the input features of raw images to generate core salient information,

$$F_q = W_q \cdot X_{rgb} + B_q, \quad (2)$$

$$F_{core} = W_f \cdot (\varepsilon(F_q \cdot F_q^T) \cdot F_q) + B_f, \quad (3)$$

where W_f and W_q are 1×1 convolution layers with respective biases B_f and B_q , and ε is a softmax function. Then the core saliency F_{core} is used to supplement information to features X_{flow} of the optical flow, whose output is

$$F_{flow} = W_{flow} \cdot (X_{flow} + F_{core}) + B_{flow}, \quad (4)$$

where W_{flow} is a 3×3 convolution layer with bias B_{flow} . We fuse F_{flow} and F_{rgb} to generate the channel-wise descriptor R_{fuse} with a sigmoid function,

$$R_{fuse} = \sigma(F_{flow} \odot F_{rgb}), \quad (5)$$

where “ \odot ” denotes element-wise multiplication. Therefore, when the main modality is raw images, the output features O_{rgb} of CSCM are defined as

$$O_{rgb} = R_{fuse} \odot X_{rgb}. \quad (6)$$

Equations 5 and 6 constitute the compensation unit for the fusion of core features and filtering of irrelevant features. Features O_{rgb} are fed into the attention generator to generate modal-specific attention scores.

When the main modality is optical flow and the auxiliary modality is raw images, the procedure is the same as above, with output features O_{flow} . The fused features of O_{rgb} and

O_{flow} are fed into the classifier to generate class-specific logits.

Video-level Distribution Consistency Strategy. Contrary to the general TAL [49], [50], [51], [52], expression spotting heavily relies on the sample distribution of different classes [10], [11]. We observe that the distribution of MEs in long, untrimmed face videos is sparser than that of MaEs on the CAS(ME)² [10] and SAMM-LV [11] datasets, because MEs are more challenging to evoke than MaEs [13]. Furthermore, the foreground occupies a smaller portion of the video compared to the background [10], [11], because emotions are frequently expressed in only a few specific (sparse) frames or intervals in a video [75]. Therefore, the difference in sample distributions facilitates the distinguishing of snippets belonging to the foreground or background in our model.

Previous WTAL frameworks [21], [22], [35], [61] have generally taken the same values in the top- K to aggregate the snippet-level temporal logits of T-CAMs along the temporal dimension for different categories and the background class, and obtain video-level temporal average logits. Compared with the above WTAL approaches with multiple classifications, WES is limited to two types, i.e., ME and MaE. Therefore, as important prior information, the distribution of MaEs and MEs can be incorporated into the model training by setting different values in the top- K to sample the logits of T-CAMs in WES. (In the snippet classification of Figure 2, some branches must consider the distribution of the background.) This strategy is defined as video-level distribution consistency in our MIL-based MC-WES framework.

We adopt the top- K temporal average pooling strategy [21], [22], [23] and the sampling rate $k_i \in \mathbb{R}^{n+1}$ for the i -th category is

$$k_i = \max(1, \lfloor \frac{T}{h_i} \rfloor), \quad (7)$$

where T is the number of snippets in Section 3.2, and the h_i are the predefined parameters to calculate the sampling rate k_i . We denote the snippet-level logits for the j -th snippet as s_{ij} in T-CAMs \mathcal{S} . Our video-level class-wise logits u_i for the i -th category of training videos is obtained by aggregating the snippet-level logits corresponding to the top- k_i values along the temporal dimension,

$$u_i = \max_{M \subset \{1, \dots, T\}, |M|=k_i} \frac{1}{k_i} \sum_{j=1}^{k_i} s_{ij}. \quad (8)$$

A softmax function is applied to obtain the video-level class confidence scores $p_i = \frac{\exp(u_i)}{\sum_{i=1}^{n+1} \exp(u_i)}$ along the class dimension, which are used to calculate the classification loss.

Label-level Duration Consistency Strategy. Many habitual and unconscious actions, such as blinking, pursing the lips, and shaking the head, constitute background intervals, which sometimes produce significant inter-frame and interval differences. Continuous foreground intervals also contain such differences due to the persistent change in the face. As the intensity and range of facial movements are difficult to quantify, previous frameworks [2], [16], [17] have chosen the durations of MaEs and MEs as classification benchmarks. MEs are shown to be challenging to learn

due to their short duration and low intensity with low confidence [2], [17].

Based on existing ME datasets, we observe that the ME intervals cover only a limited number of snippets. For example, as the durations of MEs are shorter than 0.5 second [28], if each snippet contains 8 frames, MEs can cover 2 or 3 snippets when the video is at 30 FPS. In WTAL frameworks [21], [22], [29], [35], [57], we use attention scores to measure the probability that snippets belong to the foreground intervals. Therefore, a group of snippets with a larger average attention score in a certain neighborhood range (i.e., the number of snippets covered) refers to a proposal interval. Then we can easily remove potential ME intervals based on duration by filtering deviations from the average attention scores of consecutive snippets within a neighborhood. The remaining snippets are labeled as pseudo MaE and background snippets to refine the model. We define this strategy as the label-level duration consistency with pseudo labels.

Consistent with previous research [21], [22], we utilize the guide-loss function in our MC-WES framework to assign attention scores inversely proportional to the probability of a snippet belonging to background intervals. Thus, snippets with lower confidence have a higher probability of being classified as background. To remove more potential ME snippets using less supervised information, we classify smaller deviations as intra-background and intra-MaE differences, and larger deviations as differences between the onset and offset of MaEs and the background.

We calculate the mean attention score of the j -th snippet in a certain neighborhood range as:

$$Q_j = \frac{\sum_{t=j}^{t+\eta} (\mathcal{A}_t)}{\eta}, \quad (9)$$

where \mathcal{A}_t is the snippet-level attention score for the t -th snippet, and η is the neighborhood range. Then we compute the interval-level adjacent deviation $\Delta_j = |Q_{j+1} - Q_j|$ for the j -th interval. Based on deviation filtering, we set up a mask matrix,

$$\mathcal{M}_j = \begin{cases} 0, & \text{if } \omega_l \bar{Q} < \Delta_j < \omega_u \bar{Q} \\ 1, & \text{otherwise,} \end{cases} \quad (10)$$

where \bar{Q} is the mean deviation, ω_l , and ω_u are the parameters defining the respective lower and upper bounds. When the adjacent deviation Δ_j for the j -th interval is less than $\omega_l \bar{Q}$, we can localize the background and intra-MaE intervals, and when it is greater than $\omega_u \bar{Q}$, we can localize the onset- and offset-related MaE or background intervals.

By integrating the mask matrix \mathcal{M} and class-specific T-CAMs \mathcal{S} , the logits $\tilde{\mathcal{S}} = \mathcal{M} \odot \mathcal{S}$ corresponding to the background and MaE snippets are obtained. The strategy is essentially to select the temporal attention scores of snippets that potentially belong to one or more specific categories to generate pseudo labels serving as supervised information for subsequent operations.

Segment-level Feature Consistency Strategy. As our MC-WES framework is only given with video-level supervised information, modeling the correlation between videos of the same category becomes particularly significant. Previous approaches [21], [23] only use classification-related features to compare video pairs with partially consistent labels to

reduce intra-class variation and increase inter-class variation. However, when dealing with a large number of snippets, to use a softmax function to generate probabilities by activating logits along the temporal dimension may result in over-smoothness of the results integrated with video features in a co-activity similarity loss [21], [23]. Moreover, the diversity of contexts can lead to intra-class variation, which can interfere with the computation of inter-video correlations if all features of a video pair are used.

Therefore, we utilize the top- k (here we use the sampling rate k of MaEs from Equation 7) localization-related attention scores to select corresponding classification-related features and logits to implement the segment-level feature consistency strategy in a video pair v_1 and v_2 , and compute the snippet-level similarity of the selected features of v_1 to the other features of v_2 . Each snippet-level maximum similarity of v_2 is required to match as closely as possible with the corresponding snippet-level attention score of v_2 .

We pick some videos from each batch to construct N_p video pairs $(v_{d1}, v_{d2}), d = 1, \dots, N_p$, where the labels in the two videos of each pair are at least partially the same. We treat the indexes corresponding to top- k attention scores \mathcal{A}_{d1} of video v_{d1} as guiding labels to help select logits $u'_{d1} \in \mathbb{R}^{k \times n}$ and fused features $f'_{d1} \in \mathbb{R}^{k \times D}$ from video v_{d1} in the d -th video pair. Note that the selected logits do not contain those associated with background classes. The selected logits u'_{d1} are activated separately by a softmax function along the class dimension, and integrated with the selected features f'_{d1} to obtain category-level features $f_{s_{d1}} \in \mathbb{R}^{k \times D \times n}$. The similarity $h_{d2} \in \mathbb{R}^{k \times T \times n}$ of video v_{d2} is calculated as

$$h_{d2} = \varepsilon((f_{d2} \otimes (f_{s_{d1}})^T)^T) \quad (11)$$

where “ \otimes ” denotes matrix multiplication, and $f_{d2} \in \mathbb{R}^{T \times D}$ is the feature of the video v_{d2} , to modulate the results of matrix multiplication along the top- k dimension. We select the maximum similarity ms_{d2} along the top- k dimension,

$$ms_{d2} = \max(h_{d2k}). \quad (12)$$

The maximum similarities $ms_{d2} \in \mathbb{R}^{T \times n}$ and attention scores $\mathcal{A}_{d2} \in \mathbb{R}^T$ of video v_{d2} are optimized to match as closely as possible based on the matching function cs , defined as

$$cs_{d2} = \sum_{i=1}^n \sum_{j=T}^n \frac{y_{di} \cdot \mathcal{A}_{d2j}^T \otimes ms_{d2ji}}{\sum_{j=1}^T \mathcal{A}_{d2j}}, \quad (13)$$

where $y_d = y_{d1} \odot y_{d2}$ consists of the labels of the videos of v_{d1} and v_{d2} without the background class. This similarity function is analogous to cosine similarity. When the roles of the two videos are exchanged, we can use the same workflow to obtain cs_{d1} .

3.4 Model Training

Top- K MIL Loss. As shown in Figure 2, there are three branches in snippet spotting to process the logits of T-CAMs \mathcal{S} . The first branch uses the original logits and the video-level distribution consistency strategy to produce video-level class confidence scores p_i^1 with the top- k_i in Equation

7 for the i -th category. We calculate the MIL loss in the first branch as

$$\mathcal{L}_{mil}^1 = - \sum_{i=1}^{n+1} y_i^1 \log(p_i^1), \quad (14)$$

where y_i^1 consists of the ground truth labels containing the background class, i.e., $y_{n+1}^1 = 1$.

The middle branch applies the attention score \mathcal{A} to inhibit the background snippets in T-CAMs \mathcal{S} . Then we use the video-level distribution consistency strategy to generate video-level class confidence scores p_i^2 with processed logits of T-CAMs $\hat{\mathcal{S}}$. The MIL loss of the middle branch is

$$\mathcal{L}_{mil}^2 = - \sum_{i=1}^{n+1} y_i^2 \log(p_i^2), \quad (15)$$

where y_i^2 is the ground truth label without the background class, i.e., $y_{n+1}^2 = 0$.

The third branch integrates the mask matrix \mathcal{M} generated by the label-level duration consistency strategy and the original T-CAMs \mathcal{S} to produce video-level class confidence scores p_i^3 with the video-level distribution consistency strategy. The MIL loss of this branch is defined as:

$$\mathcal{L}_{mil}^3 = - \sum_{i=1}^{n+1} y_i^3 \log(p_i^3), \quad (16)$$

where y_i^3 represents the ground truth labels with the background class and without ME class.

Attention-guided Feature Consistency Loss. To merge localization and classification information, the segment-level feature consistency strategy is designed to calculate the similarity cs_{d1} and cs_{d2} for the d -th pair of videos. Accordingly, we assume that for a video pair, some video-level labels are present in both videos as valid labels (without the background class). Then we count the number of valid labels N_s across all video pairs in a batch. Accordingly, the attention-guided feature consistency loss is calculated as:

$$\mathcal{L}_c = 1 - \frac{1}{2N_s} \sum_{d=1}^{N_p} (cs_{d1} + cs_{d2}). \quad (17)$$

where N_p is the total number of all video pairs.

Final Joint Loss. Following previous works [21], [22], our MC-WES framework uses the guide and sparsity loss functions. The goal of the former is to make the attention score inverse to the probability that a snippet belongs to the background. We first calculate the probability of a snippet being in foreground intervals,

$$p_f = 1 - p_{(n+1)}, \quad (18)$$

where $p_{(n+1)}$ is the probability of a snippet belonging to the background class. Then the guide loss function is

$$\mathcal{L}_{guide} = \frac{1}{3T} (\|p_f - \mathcal{A}\|_1 + \|p_f - \mathcal{A}_{rgb}\|_1 + \|p_f - \mathcal{A}_{flow}\|_1), \quad (19)$$

where $\|\cdot\|_1$ is the L1-norm function, \mathcal{A}_{rgb} and \mathcal{A}_{flow} are respectively the attention scores of the snippets of raw images and optical flow, and \mathcal{A} is the snippet-level mean of \mathcal{A}_{rgb} and \mathcal{A}_{flow} .

The sparsity loss function is based on the observation that the positive samples are sparsely distributed in a long

video [54]. In our framework, we utilize the L1-norm to implement the sparsity loss function as,

$$\mathcal{L}_{sparse} = \frac{1}{3T} (\|\mathcal{A}\|_1 + \|\mathcal{A}_{rgb}\|_1 + \|\mathcal{A}_{flow}\|_1). \quad (20)$$

We follow CO₂-Net [21] to apply mutual learning loss on two modal-specific attention scores with the mean square error (MSE) function,

$$\mathcal{L}_{ml} = \frac{1}{2T} (\|\mathcal{A}_{rgb} - \rho(\mathcal{A}_{flow})\|_2^2 + \|\rho(\mathcal{A}_{rgb}) - \mathcal{A}_{flow}\|_2^2). \quad (21)$$

where $\rho(\cdot)$ is the gradient detachment function and $\|\cdot\|_2$ is the L2-norm function.

Finally, we combine the above loss functions to form the final optimization function for the whole framework,

$$\mathcal{L} = \mathcal{L}_{mil}^1 + \mathcal{L}_{mil}^2 + \lambda_1 \mathcal{L}_{mil}^3 + \lambda_2 \mathcal{L}_c + \lambda_3 \mathcal{L}_{sparse} + \lambda_4 \mathcal{L}_{guide} + \mathcal{L}_{ml}, \quad (22)$$

where $\lambda_1, \lambda_2, \lambda_3,$ and λ_4 are predefined hyperparameters.

3.5 Expression Spotting

During testing, previous works [21], [22] set upper and lower bounds, τ_u and τ_l , respectively, along with level N_l to produce a one-dimensional vector m_t , uniformly divided between τ_u and τ_l , and then select a threshold from the threshold vector m_t to filter the continuous temporal attention scores, which are used to localize class-agnostic video snippets. Instead, we apply a range of consecutive values to build a multiple top- k vector, each value of which is utilized to filter the continuous temporal attention scores to localize class-agnostic video snippets. This aims to generate a higher F1-score that we are concerned with both recall and precision, thus, expression proposals that are of the highest possibility need to be selected. Following AutoLoc [71], we sort the snippets based on their timestamps in the video, and aggregate snippets corresponding to successive timestamps into a series of video interval proposals $[f_{on}, f_{off}]$, with varying durations. To spot short-duration intervals and generate as few proposals as possible, we set 15 consecutive k values with an interval of 1 in the multiple top- k vector, similar to a multi-threshold strategy. We define the duration of the i -th proposal as $dp_i = f_{on}^i - f_{off}^i + 1$, and calculate the class-specific score ϕ_{ij} for the j -th category with the suppressed T-CAMs $\hat{\mathcal{S}}$,

$$\phi_{ij} = \phi_{ij}^{inner} - \phi_{ij}^{outer} + \varsigma p_{ij}. \quad (23)$$

$$\phi_{ij}^{inner} = \frac{1}{dp_i} \sum_{t=f_{on}^i}^{f_{off}^i} s_{ijt}, \quad (24)$$

$$\phi_{ij}^{outer} = \frac{1}{2\psi dp_i} \left(\sum_{t=f_{on}^i - \psi dp_i}^{f_{on}^i} s_{ijt} + \sum_{t=f_{off}^i}^{f_{off}^i + \psi dp_i} s_{ijt} \right), \quad (25)$$

where ς is a hyperparameter related to the probability of one proposal, p_{ij} is the video-level class score for the j -th category, s_{ijt} is the snippet-level class logit for the j -th category, ψ is a hyperparameter related to the duration of a proposal, ϕ_{ij}^{inner} is the inner class logit for the j -th category, i.e., the mean logit from timestamp f_{on}^i and f_{off}^i , and ϕ_{ij}^{outer} is the outer class logit for the j -th category, which is from

the mean of the corresponding logits after expanding ψdp_i timestamps since f_{on}^i towards the start of the video and f_{off}^i towards the end of the video, respectively. The essence of the class-specific score ϕ_{ij} for the j -th category is the outer-inner score of AutoLoc [71].

Because there are two types of expressions, each proposal generated by the attention scores has two class-specific scores. Thus, we process all $2n_e$ generated expression proposals $(f_{on}^{ij}, f_{off}^{ij}, y_{ij}, \phi_{ij})$, where $i = 1, \dots, n_e$ and $j = 1, \dots, n$, using non-maximum suppression (NMS) [76] to eliminate redundant proposals.

4 EXPERIMENTS

4.1 Datasets

We evaluate our MC-WES framework on two popular spotting datasets: CAS(ME)² [10] and SAMM-LV [11]. CAS(ME)² dataset consists of 98 long videos at 30 FPS, each with an average of 2940 frames and 96% background, annotated with 57 MEs and 300 MaEs from 22 subjects. SAMM-LV dataset consists of 224 long videos at 200 FPS, each with an average of 7000 frames and 68% background, annotated with 159 MEs and 340 MaEs from 32 subjects.

4.2 Evaluation Metrics

We employ the intersection over union (IoU) method to select eligible expression proposals that are defined as true positive (TP) samples. The IoU between a spotted proposal E_s and a ground truth interval E_{gt} is calculated as:

$$\frac{E_s \cap E_{gt}}{E_s \cup E_{gt}} \geq k_{eval}, \quad (26)$$

where k_{eval} is the evaluation threshold, which is commonly set to 0.5 for expression spotting [17].

According to the metrics used in the Micro-Expression Grand Challenge (MEGC) 2019 [77], we need to calculate F1-scores for all proposals, and for MaEs and MEs. However, considering that the maximum duration of an ME is 0.5 second [28] and k_{eval} in Equation 26 is 0.5, we calculate the F1-scores for proposals with durations below 15 and 30 frames on the CAS(ME)² dataset, and below 100 and 200 frames on the SAMM-LV dataset. Following previous work [16], we also calculate the F1-score by selecting proposals whose durations are less than 0.5 second from those corresponding to the best overall F1-score as the ME proposals. In summary, we calculate three versions of the F1-score for MEs, defined as F1-ME(0.5), F1-ME(1.0), and F1-ME(p). F1-ME(0.5) and F1-ME(1.0) are determined for ME proposals belonging to the sets with durations shorter than 0.5 and 1.0 second, respectively, and F1-ME(p) is determined for all ME proposals from the set corresponding to the optimal overall F1-score and shorter than 0.5 second. F1-ME(p) and F1-ME(0.5) are employed to assess whether all ME TP samples in the overall proposal set are present in the optimal proposal set. If F1-ME(p) and F1-ME(0.5) are close, it indicates that the model can spot not only the majority of TP samples but also the majority of ME TP samples.

4.3 Implementation Details

On the CAS(ME)² dataset, we sample every continuous nonoverlapping 8 frames as a snippet to split each video and optical flow, and on the SAMM-LV dataset, we take a fix duration of 32 frames as a snippet. Then we apply the I3D model to extract 1024-dimension features for each snippet. During training, we randomly sample 250 and 380 snippets for each video of the CAS(ME)² and SAMM-LV dataset, respectively. During testing, we take all snippets for each video.

We use Adam [78] as the optimizer, and train the model with 1000 iterations for each dataset. The batch size is set to 10. In each batch, six videos are used to construct three video pairs to implement the segment-level feature consistency strategy. For CAS(ME)², we set $\lambda_1 = \lambda_2 = 0.5$, $\lambda_3 = \lambda_4 = 0.8$, $\omega_l = 1.2$, $\omega_u = 1.4$, a learning rate of 0.0005 during training, and $\varsigma = 0.15$ and $\psi = 0.25$ during testing. For SAMM-LV, we set $\lambda_1 = \lambda_2 = 0.5$, $\lambda_3 = \lambda_4 = 0.7$, $\omega_l = 1.5$, $\omega_u = 1.8$ and a learning rate of 0.0008 during training, and $\varsigma = 0.50$ and $\psi = 0.25$ during testing. To remove redundant proposals, we use Non-Maximum Suppression (NMS) [76] on both datasets, with a threshold of 0.01. When we calculate the precision and recall rates, we determine classes based on the temporal duration of proposals [77].

TABLE 1

Performances with different multi-modal feature fusion methods on the CAS(ME)² dataset.

Measure	Fusion Method		
	Concatenate	CCM	CSCM
F1-ME(0.5)	0.118	0.141	0.167
F1-ME(1.0)	0.091	0.092	0.108
F1-ME(p)	0.034	0.114	0.169
Recall	0.143	0.202	0.266
Precision	0.378	0.283	0.415
F1-score	0.207	0.236	0.324

TABLE 2

Performances with different multi-modal feature fusion methods on the SAMM-LV dataset.

Measure	Fusion Method		
	Concatenate	CCM	CSCM
F1-ME(0.5)	0.110	0.097	0.135
F1-ME(1.0)	0.048	0.040	0.055
F1-ME(p)	0.093	0.048	0.135
Recall	0.218	0.216	0.263
Precision	0.136	0.172	0.178
F1-score	0.168	0.192	0.212

4.4 Ablation Study

We utilize the leave-one-subject-out (LOSO) learning strategy to train our model and generate proposals. After training, we use a truncation threshold of 0.1 to remove samples with confidence below this threshold, and calculate the recall rate, precision rate, and F1-score based on the remaining proposals on the CAS(ME)² and SAMM-LV datasets.

TABLE 3

Performances with different top- K temporal average pooling strategy on the CAS(ME)² and SAMM-LV datasets. “ h ” is the predefined parameters in Equation 7.

h	CAS(ME) ²						SAMM-LV					
	F1-ME(0.5)	F1-ME(1.0)	F1-ME(p)	Recall	Precision	F1-score	F1-ME(0.5)	F1-ME(1.0)	F1-ME(p)	Recall	Precision	F1-score
[5, 5, 5]	0.034	0.034	0.027	0.109	0.361	0.168	0.107	0.043	0.074	0.234	0.159	0.189
[7, 7, 7]	0.066	0.057	0.029	0.118	0.400	0.182	0.110	0.043	0.055	0.238	0.162	0.193
[9, 9, 9]	0.034	0.034	0.028	0.112	0.444	0.179	0.098	0.046	0.066	0.242	0.178	0.205
[5, 7, 5]	0.141	0.092	0.114	0.202	0.283	0.236	0.097	0.040	0.048	0.216	0.172	0.192
[7, 7, 5]	0.141	0.092	0.114	0.202	0.283	0.236	0.097	0.040	0.048	0.216	0.172	0.192
[5, 9, 5]	0.138	0.111	0.033	0.179	0.379	0.243	0.111	0.044	0.0	0.220	0.180	0.198
[7, 9, 5]	0.167	0.108	0.169	0.266	0.415	0.324	0.135	0.055	0.135	0.263	0.178	0.212

TABLE 4

Performances with different durations of snippets on the CAS(ME)² and SAMM-LV datasets.

Measure	Duration					
	CAS(ME) ²			SAMM-LV		
	4	8	16	16	32	48
F1-ME(0.5)	0.110	0.167	0.0	0.174	0.135	0.105
F1-ME(1.0)	0.080	0.108	0.0	0.056	0.055	0.057
F1-ME(p)	0.083	0.169	0.0	0.118	0.135	0.088
RecaLL	0.152	0.266	0.129	0.194	0.263	0.212
Precision	0.346	0.415	0.189	0.134	0.178	0.162
F1-score	0.211	0.324	0.153	0.159	0.212	0.184

4.4.1 Effect of Modal-level Consistency

To alleviate the modal-level information discrepancy from the raw image and optical flow, we train our model on the CAS(ME)² and SAMM-LV datasets using different multi-modal feature fusion methods, including direct concatenating, CCM [21], and our proposed CSCM with the same configuration.

The results of Table 1 and 2 show that CSCM can significantly improve the recall rate, precision rate, and F1-score of the model on both datasets compared with previous methods such as direct concatenating and CCM. In particular, compared with direct concatenating, CCM improves ME and MaE spotting, but the improvement by CSCM is more significant. These results suggest that a network derived from video action recognition, e.g., I3D, may produce information redundancy in the extracted features that affects the learning of the spotting model. Moreover, inter-modal consensus modules like CCM can help eliminate redundant information and improve results, but there is still inter-modal feature inconsistency, which may degrade the model’s performance. In contrast, our proposed CSCM effectively removes information redundancy and enables modal-level consistency to alleviate inter-modal gaps.

On both datasets, our proposed CSCM leads to a noticeable increase in the spotting results of MEs over CCM and direct concatenation, which cannot make the proposals with the optimal F1-score contain the most MEs, with the result that F1-ME(p) is not close to F1-ME(0.5) or much larger than F1-ME(1.0). With CSCM, the best result of F1-ME(0.5) is equal to F1-ME(p) and much larger than F1-ME(1.0) on the two datasets, indicating that it can contribute meaningfully

to capturing the most MEs in the proposals.

4.4.2 Hyperparameters in Video-level Consistency

To merge the prior about the distribution information of different categories, we adopt a video-level distribution consistency strategy with different values to achieve the top- K temporal average pooling strategy in our MIL-based framework, to calculate the average logits of different classes to obtain the final classification loss. Therefore, we set various combinations of values in h to calculate the sampling rate for different categories using Equation 7. For example, with a combination [5, 5, 5] in h , the first two values are used to calculate the sampling rate of the MaE and ME logits, respectively, and the last to calculate the sampling rate of the background logits.

The results of Table 3 show that computing the average logits with the same values (i.e., [5, 5, 5], [7, 7, 7], [9, 9, 9]) for different categories and the background class in the MIL-based framework reduces the spotting capability of the model, whereas our strategy with different values in h (i.e., [7, 9, 5]) achieves better results. Xu et. al [75] points out that most of the frames belong to the background, which is also observed in Section 4.1. Therefore, the background value in h must be set to the minimum to ensure that most of the background logits are retained for the calculation of the average logits. Moreover, since MEs are distributed more sparsely than MaEs [10], [11], the value of MaE is lower than that of ME in h . Using the same part of the values of h (i.e., [5, 7, 5], [7, 7, 5], [5, 9, 5]) does not significantly improve the results of our spotting model, which shows that our video-level distribution consistency strategy of setting different values based on the distribution (i.e., [7, 9, 5]) is valid.

In addition, our strategy, which utilizes different values in h (i.e., [7, 9, 5]), is evidently more effective in ME spotting. Other configurations of values in h (such as [5, 5, 5], [7, 7, 7], [9, 9, 9], [5, 7, 5], [7, 7, 5], and [5, 9, 5]) besides our strategy (i.e., [7, 9, 5]) lead to a decrease in F1-ME(p) compared to F1-ME(0.5), and in certain situations, F1-ME(p) is even lower than F1-ME(1.0) on both datasets. This variance in results may be attributed primarily to our setting of values based on the actual distribution of the three categories (i.e., ME, MaE, and background). Hence we establish values in h using a video-level distribution consistency strategy that can capture the majority of ME TP samples to boost the results of F1-ME(p) in the optimal proposal set, making it almost equivalent to F1-ME(0.5) in

TABLE 5
Ablation studies of our model for MaE and ME spotting on the CAS(ME)² dataset with different combinations of loss.

EXP	\mathcal{L}_{mil}^1	\mathcal{L}_{mil}^2	\mathcal{L}_{mil}^3	\mathcal{L}_c	\mathcal{L}_{sparse}	\mathcal{L}_{guide}	\mathcal{L}_{ml}	F1-ME(0.5)	F1-ME(1.0)	F1-ME(p)	Recall	Precision	F1-score
1	✓				✓	✓	✓	0.0	0.0	0.0	0.020	0.117	0.034
2		✓			✓	✓	✓	0.062	0.043	0.034	0.070	0.092	0.079
3	✓	✓			✓	✓	✓	0.113	0.068	0.058	0.199	0.183	0.191
4	✓		✓		✓	✓	✓	0.0	0.0	0.0	0.025	0.113	0.041
5	✓			✓	✓	✓	✓	0.0	0.0	0.0	0.034	0.194	0.057
6	✓	✓	✓		✓	✓	✓	0.091	0.063	0.036	0.157	0.220	0.183
7	✓	✓		✓	✓	✓	✓	0.121	0.076	0.057	0.154	0.342	0.212
8	✓		✓	✓	✓	✓	✓	0.034	0.034	0.0	0.048	0.165	0.074
9	✓	✓	✓	✓	✓	✓	✓	0.167	0.108	0.169	0.266	0.415	0.324

TABLE 6
Performances with different post-processing on the CAS(ME)² and SAMM-LV datasets.

Measure	Post-processing			
	CAS(ME) ²		SAMM-LV	
	top_k	threshold	top_k	threshold
F1-ME(0.5)	0.167	0.078	0.135	0.092
F1-ME(1.0)	0.108	0.069	0.057	0.050
F1-ME(p)	0.169	0.028	0.135	0.078
Recall	0.266	0.162	0.263	0.206
Precision	0.415	0.152	0.178	0.150
F1-score	0.324	0.157	0.212	0.173

the overall proposal set, and significantly greater than F1-ME(1.0) in the overall proposal set on both datasets.

4.4.3 Effect of Different Snippet Durations

We investigate the effect of different snippet durations on model training. It is clear that the longer each snippet is, the fewer snippets are sampled from a video. In addition, because each snippet is represented as 1024-dimensional features extracted by the I3D model, fewer snippets in one video cannot learn fine-grained information, while too many may introduce too much noise. Note that in order to avoid mutual interference between neighboring snippets, each video in this paper is segmented into a sequence of non-overlapping snippets. Here, we test snippet durations of 4, 8, and 16 for CAS(ME)², and 16, 32, and 48 for SAMM-LV, respectively, during model training, and we keep the same settings during testing.

Table 4 shows that the optimal snippet durations in terms of numbers of frames for CAS(ME)² and SAMM-LV are 8 and 16, respectively. A snippet duration that is either too long or too short reduces the spotting capability of our spotting model. This means that too short of a snippet duration may introduce too much noisy information, while a too long duration may lose sensitivity to short MEs. In particular, longer snippet durations greatly inhibit ME spotting on the two datasets, even on the CAS(ME)² dataset, where the model is unable to spot MEs when the duration is 16. The above results suggest that the snippet duration should not be close to or exceed the maximum duration of the MEs in order to prevent loss of important information, nor be too small to avoid introducing excessive noise.

4.4.4 Effect of Loss Function

Each component of the loss function in Equation 22 plays a specific role in refining our model. To verify the effectiveness of each component, we adopt various combinations of them in the loss functions to train our model under the same configuration. We test the importance of four components: \mathcal{L}_{mil}^1 , \mathcal{L}_{mil}^2 , \mathcal{L}_{mil}^3 , and \mathcal{L}_c . Specifically, compared with CO₂-Net [21], we add \mathcal{L}_{mil}^3 to learn pure features of MaE, and replace the co-activity similarity loss with our attention-guided feature consistency loss \mathcal{L}_c .

Table 5 shows that \mathcal{L}_{mil}^2 plays a more significant role than \mathcal{L}_{mil}^1 in the MIL-based framework in generating accurate predictions, especially for MEs. In addition, combining \mathcal{L}_{mil}^1 and \mathcal{L}_{mil}^2 can noticeably increase the spotting capability of our model compared with each one alone. The overall improvement (F1-score) is significantly greater than that for ME spotting (F1-ME), which indicates that the improvement from \mathcal{L}_{mil}^1 and \mathcal{L}_{mil}^2 preferentially improves MaE spotting. Adding \mathcal{L}_{mil}^3 has no effect on improving spotting results, whereas adding \mathcal{L}_c increases the F1-score by 2%. Adding either \mathcal{L}_{mil}^3 or \mathcal{L}_c does not improve the spotting of MEs. When added with \mathcal{L}_{mil}^3 and \mathcal{L}_c , the lack of \mathcal{L}_{mil}^2 decreases the performance enormously. The use of all four components together remarkably improves the performance of ME spotting and overall spotting. The above results also demonstrate the effect of our proposed label-level duration consistency strategy and segment-level feature consistency strategy.

4.4.5 Effect of Different Post-processing

Previous works [21], [22] has generally employed a multi-threshold approach based on attention scores to select snippets for generating proposals, which are then used to calculate the mean average precision (mAP). To accurately assess the localization capability of the model, the TAL task tends to calculate mAP under various intersection over union (IoU) thresholds. These results on mAP can adequately reflect the impact of different confidence counterparts on the proposal results. However, the spotting task favors the use of a certain confidence threshold to filter proposals and calculate metrics. Once we use a multi-threshold approach to filter attention scores and generate proposals, a large number of negative samples will be produced.

To address this issue, our model uses a top_k approach to select a limited number of snippets to generate proposals, only filtering snippets with high attention values

TABLE 7
Comparison with the fully-supervised state-of-the-art models on the CAS(ME)² dataset.

Supervision	Method	F1-ME(0.5)	F1-ME(1.0)	F1-ME(p)	Recall	Precision	F1-score
Full	He [79]	-	-	0.008	0.020	0.364	0.038
	Zhang [80]	-	-	0.055	0.085	0.406	0.140
	MESNet [2]	-	-	-	-	-	0.036
	Yap [39]	-	-	0.012	-	-	0.030
	LSSNet [17]	-	-	0.063	-	-	0.327
	He [81]	-	-	0.197	-	-	0.343
	MTSN [82]	-	-	0.081	0.342	0.385	0.362
	Zhao [83]	-	-	-	-	-	0.403
Weak	MC-WES	0.167	0.108	0.169	0.266	0.415	0.324

TABLE 8
Comparison with the fully-supervised state-of-the-art models on the SAMM-LV dataset.

Supervision	Method	F1-ME(0.5)	F1-ME(1.0)	F1-ME(p)	Recall	Precision	F1-score
Full	He [79]	-	-	0.036	0.029	0.101	0.045
	Zhang [80]	-	-	0.073	0.079	0.136	0.100
	MESNet [2]	-	-	-	-	-	0.088
	Yap [39]	-	-	0.044	-	-	0.119
	LSSNet [17]	-	-	0.218	-	-	0.290
	He [81]	-	-	0.216	-	-	0.364
	MTSN [82]	-	-	0.088	0.260	0.319	0.287
	Zhao [83]	-	-	-	-	-	0.386
Weak	MC-WES	0.135	0.055	0.135	0.263	0.178	0.212

and aggregating them into proposals. As we mentioned in Section 3.5, since the videos on the CAS(ME)² and SAMM-LV datasets have different durations, with different numbers of snippets belonging to the foreground, we leverage the segment-level feature consistency strategy to generate class-agnostic proposals based on the predefined parameter from the multiple top- k vector. Subsequently, the category scores for these proposals are calculated according to the procedure described in Section 3.5. Because h is predefined as [7, 9, 5] for CAS(ME)², we set the start parameter $k_0 = 8$ in the multiple top- k vector for a compromise between MEs and MaEs when training our model on the CAS(ME)² dataset. As the duration of the snippets on the SAMM-LV dataset is shorter than that on the CAS(ME)² dataset, to spot more proposals, we set $k_0 = 2$ in the multiple top- k vector when training our model on the SAMM-LV dataset.

The results of Table 6 show that our top_k approach is better than the multi-threshold approach in terms of recall, precision, and F1-score. This indicates that our model can spot more accurate snippets and produce fewer negative samples. The multi-threshold approach primarily shows a declining precision rate in addition to reducing the recall rate due to the large number of negative samples generated during testing. As for ME spotting, the performance reduction by the multi-threshold approach is remarkable on both datasets. On the CAS(ME)² dataset, F1-ME(P) is 0.028, which is close to zero, suggesting that most MEs fail to be spotted using this approach on this dataset.

4.5 Comparison with State-of-the-art Methods

To the best of our knowledge, ours is the first attempt to use weakly-supervised video-level labels to achieve frame-level

expression spotting. Therefore, we can only compare MC-WES with recent fully-supervised state-of-the-art methods on the CAS(ME)² and SAMM-LV datasets, so as to indirectly verify the model’s potential.

Table 7 shows that our proposed weakly-supervised MC-WES can achieve results that are to some extent comparable to the representative fully-supervised methods on the CAS(ME)² dataset. There is not much performance degradation in the spotting of MEs. Compared with MTSN [82], MC-WES obtains an improved recall rate on the CAS(ME)² dataset. Table 8 indicates that our method also achieves acceptable results on the SAMM-LV dataset. Compared with MTSN [82], MC-WES needs improvement in terms of the precision rate on the SAMM-LV dataset. The above situations occur because a denser sample distribution and greater variation in sample duration exist on the SAMM-LV dataset, as seen in Section 4.1. For example, some ground truth intervals on the SAMM-LV dataset are longer than 20.0 seconds, which clearly contradicts Ekman’s observation that the conventional duration of MaEs is within 4.0 seconds [4]. In contrast, the CAS(ME)² dataset does not contain ground truth intervals that last longer than 4.0 seconds. Considering that there are few ground truth intervals for SAMM-LV, we did not remove those long-tail intervals. This may also worsen spotting on the SAMM-LV dataset.

5 CONCLUSION

In this paper, to avoid the requirement of tedious frame-level labeling for the ME datasets, we explored the use of a weakly-supervised video-level MIL-based framework, MC-WES, to spot frame-level expressions using multi-

consistency collaborative mechanisms, including the strategies of modal-level saliency, video-level distribution, label-level duration, and segment-level feature consistencies, to alleviate inter-modal, inter-sample, and inter-task gaps. The modal-level saliency consistency strategy is utilized to capture the key correlations between raw images and optical flow. The video-level distribution consistency strategy merges information of different sparsities in the sample distribution, and the label-level duration consistency strategy exploits the difference in duration of facial muscles. To learn more representational features and mitigate the discrepancy between classification and localization, we employ the segment-level feature consistency strategy. Extensive experiments on the CAS(ME)² and SAMM-LV datasets are conducted to validate MC-WES, and the results of the ablation experiments demonstrate that the proposed multi-consistency collaborative mechanism enables our weakly-supervised spotting method to achieve results comparable to those of fully-supervised spotting methods.

Although the MC-WES framework relies on confidence to select proposals and then calculate precision and recall rates, we believe that mAP is a more appropriate metric to evaluate the spotting capability of the model. As an important future work, we plan to develop a more refined framework to enhance the model's robustness of expression spotting when there exist a possible bias in labeling and large-scale duration of ground truth intervals inevitably, such as those on the SAMM-LV dataset.

ACKNOWLEDGMENTS

This work was supported by STI2030-Major Projects (#2022ZD0204600), Sichuan Science and Technology Program (2022ZYD0112) and the Natural Science Foundation of Sichuan Province (2023NSFSC0640).

REFERENCES

- [1] P. Ekman and W. V. Friesen, "Nonverbal leakage and clues to deception," *Psychiatry*, vol. 32, no. 1, pp. 88–106, 1969.
- [2] S. Wang, Y. He, J. Li, and X. Fu, "MESNet: A convolutional neural network for spotting multi-scale micro-expression intervals in long videos," *IEEE Trans. Image Process.*, vol. 30, pp. 3956–3969, 2021.
- [3] M. Frank, M. Herbasz, K. Sinuk, A. Keller, and C. Nolan, "I see how you feel: Training laypeople and professionals to recognize fleeting emotions," in *Proc. Annu. Meet. Int. Commun. Assoc., New York City*, 2009, pp. 1–35.
- [4] P. Ekman, "Darwin, deception, and facial expression," *Ann. New York Acad. Sci.*, vol. 1000, no. 1, pp. 205–221, 2003.
- [5] P. Ekman, "Lie catching and microexpressions," *The philosophy of deception*, vol. 1, no. 2, p. 5, 2009.
- [6] W. Xie, L. Shen, and J. Duan, "Adaptive weighting of handcrafted feature losses for facial expression recognition," *IEEE Trans. Cybern.*, vol. 51, no. 5, pp. 2787–2800, 2021.
- [7] S. Du, Y. Tao, and A. M. Martínez, "Compound facial expressions of emotion," *Proc. Natl. Acad. Sci. USA*, vol. 111, no. 15, pp. E1454–E1462, 2014.
- [8] S. Li, W. Deng, and J. Du, "Reliable crowdsourcing and deep locality-preserving learning for expression recognition in the wild," in *CVPR*. IEEE Computer Society, 2017, pp. 2584–2593.
- [9] L. Liang, C. Lang, Y. Li, S. Feng, and J. Zhao, "Fine-grained facial expression recognition in the wild," *IEEE Trans. Inf. Forensics Secur.*, vol. 16, pp. 482–494, 2021.
- [10] F. Qu, S. Wang, W. Yan, H. Li, S. Wu, and X. Fu, "CAS(ME)²: A database for spontaneous macro-expression and micro-expression spotting and recognition," *IEEE Trans. Affect. Comput.*, vol. 9, no. 4, pp. 424–436, 2018.
- [11] C. H. Yap, C. Kendrick, and M. H. Yap, "SAMM long videos: A spontaneous facial micro- and macro-expressions dataset," in *FG*. IEEE, 2020, pp. 771–776.
- [12] X. Ben, Y. Ren, J. Zhang, S. Wang, K. Kpalma, W. Meng, and Y. Liu, "Video-based facial micro-expression analysis: A survey of datasets, features and algorithms," *IEEE Trans. Pattern Anal. Mach. Intell.*, vol. 44, no. 9, pp. 5826–5846, 2022.
- [13] J. Li, Z. Dong, S. Lu, S.-J. Wang, W.-J. Yan, Y. Ma, Y. Liu, C. Huang, and X. Fu, "CAS(ME)³: A third generation facial spontaneous micro-expression database with depth information and high ecological validity," *IEEE Trans. Pattern Anal. Mach. Intell.*, 2022.
- [14] P. Ekman, "Facial expression and emotion," *American Psychologist*, vol. 48, pp. 384–392, 1993.
- [15] A. Esposito, "The amount of information on emotional states conveyed by the verbal and nonverbal channels: Some perceptual data," in *Progress in nonlinear speech processing*. Springer, 2007, pp. 249–268.
- [16] Y. He, "Research on micro-expression spotting method based on optical flow features," in *ACM Multimedia*. ACM, 2021, pp. 4803–4807.
- [17] W. Yu, J. Jiang, and Y. Li, "Lssnet: A two-stream convolutional neural network for spotting macro- and micro-expression in long videos," in *ACM Multimedia*. ACM, 2021, pp. 4745–4749.
- [18] M. Bartlett, G. Littlewort, J. Whitehill, E. Vural, T. Wu, K. Lee, A. Erçil, M. Cetin, and J. Movellan, "Insights on spontaneous facial expressions from automatic expression measurement," *Dynamic faces: Insights from experiments and computation*, pp. 211–238, 2010.
- [19] O. Maron and T. Lozano-Pérez, "A framework for multiple-instance learning," in *NIPS*. The MIT Press, 1997, pp. 570–576.
- [20] J. Carreira and A. Zisserman, "Quo vadis, action recognition? A new model and the kinetics dataset," in *CVPR*. IEEE Computer Society, 2017, pp. 4724–4733.
- [21] F. Hong, J. Feng, D. Xu, Y. Shan, and W. Zheng, "Cross-modal consensus network for weakly supervised temporal action localization," in *ACM Multimedia*. ACM, 2021, pp. 1591–1599.
- [22] A. Islam, C. Long, and R. J. Radke, "A hybrid attention mechanism for weakly-supervised temporal action localization," in *AAAI*. AAAI Press, 2021, pp. 1637–1645.
- [23] S. Paul, S. Roy, and A. K. Roy-Chowdhury, "W-TALC: weakly-supervised temporal activity localization and classification," in *ECCV (4)*, ser. Lecture Notes in Computer Science, vol. 11208. Springer, 2018, pp. 588–607.
- [24] B. He, X. Yang, L. Kang, Z. Cheng, X. Zhou, and A. Shrivastava, "Asm-loc: Action-aware segment modeling for weakly-supervised temporal action localization," in *CVPR*. IEEE, 2022, pp. 13915–13925.
- [25] K. Simonyan and A. Zisserman, "Two-stream convolutional networks for action recognition in videos," in *NIPS*, 2014, pp. 568–576.
- [26] L. Sevilla-Lara, Y. Liao, F. Güney, V. Jampani, A. Geiger, and M. J. Black, "On the integration of optical flow and action recognition," in *GCPR*, ser. Lecture Notes in Computer Science, vol. 11269. Springer, 2018, pp. 281–297.
- [27] Z. Li, Y. Ge, J. Yu, and Z. Chen, "Forcing the whole video as background: An adversarial learning strategy for weakly temporal action localization," in *ACM Multimedia*. ACM, 2022, pp. 5371–5379.
- [28] P. Ekman, "Emotions revealed: recognizing faces and feelings to improve communication and emotional life," *NY: OWL Books*, 2007.
- [29] D. Liu, T. Jiang, and Y. Wang, "Completeness modeling and context separation for weakly supervised temporal action localization," in *CVPR*. Computer Vision Foundation / IEEE, 2019, pp. 1298–1307.
- [30] Z. Liu, L. Wang, W. Tang, J. Yuan, N. Zheng, and G. Hua, "Weakly supervised temporal action localization through learning explicit subspaces for action and context," in *AAAI*. AAAI Press, 2021, pp. 2242–2250.
- [31] Z. Liu, L. Wang, Q. Zhang, W. Tang, J. Yuan, N. Zheng, and G. Hua, "Acenet: Action-context separation network for weakly supervised temporal action localization," in *AAAI*. AAAI Press, 2021, pp. 2233–2241.
- [32] L. Huang, L. Wang, and H. Li, "Weakly supervised temporal action localization via representative snippet knowledge propagation," in *CVPR*. IEEE, 2022, pp. 3262–3271.
- [33] W. Wang, D. Tran, and M. Feiszli, "What makes training multi-modal classification networks hard?" in *CVPR*. Computer Vision Foundation / IEEE, 2020, pp. 12692–12702.

- [34] L. Yang, J. Han, T. Zhao, N. Liu, and D. Zhang, "Structured attention composition for temporal action localization," *CoRR*, vol. abs/2205.09956, 2022.
- [35] P. Lee, Y. Uh, and H. Byun, "Background suppression network for weakly-supervised temporal action localization," in *AAAI*. AAAI Press, 2020, pp. 11320–11327.
- [36] P. Lee, J. Wang, Y. Lu, and H. Byun, "Weakly-supervised temporal action localization by uncertainty modeling," in *AAAI*. AAAI Press, 2021, pp. 1854–1862.
- [37] H. Pan, L. Xie, and Z. Wang, "Local bilinear convolutional neural network for spotting macro- and micro-expression intervals in long video sequences," in *FG*. IEEE, 2020, pp. 749–753.
- [38] Z. Zhang, T. Chen, H. Meng, G. Liu, and X. Fu, "SMEConvNet: A convolutional neural network for spotting spontaneous facial micro-expression from long videos," *IEEE Access*, vol. 6, pp. 71143–71151, 2018.
- [39] C. H. Yap, M. H. Yap, A. K. Davison, C. Kendrick, J. Li, S. Wang, and R. Cunningham, "3d-cnn for facial micro- and macro-expression spotting on long video sequences using temporal oriented reference frame," pp. 7016–7020, 2022.
- [40] G. Liong, J. See, and L. Wong, "Shallow optical flow three-stream CNN for macro- and micro-expression spotting from long videos," in *ICIP*. IEEE, 2021, pp. 2643–2647.
- [41] B. Sun, S. Cao, J. He, and L. Yu, "Two-stream attention-aware network for spontaneous micro-expression movement spotting," in *ICSESS*. IEEE, 2019, pp. 702–705.
- [42] T. Tran, Q. Vo, X. Hong, and G. Zhao, "Dense prediction for micro-expression spotting based on deep sequence model," *Electronic Imaging*, vol. 2019, no. 8, pp. 401–1, 2019.
- [43] M. Verburg and V. Menkovski, "Micro-expression detection in long videos using optical flow and recurrent neural networks," in *FG*. IEEE, 2019, pp. 1–6.
- [44] M. Zhang, Y. Zhou, J. Zhao, Y. Man, B. Liu, and R. Yao, "A survey of semi- and weakly supervised semantic segmentation of images," *Artif. Intell. Rev.*, vol. 53, no. 6, pp. 4259–4288, 2020.
- [45] W. Ge, S. Yang, and Y. Yu, "Multi-evidence filtering and fusion for multi-label classification, object detection and semantic segmentation based on weakly supervised learning," in *CVPR*. Computer Vision Foundation / IEEE Computer Society, 2018, pp. 1277–1286.
- [46] A. Vezhnevets, V. Ferrari, and J. M. Buhmann, "Weakly supervised semantic segmentation with a multi-image model," in *ICCV*. IEEE Computer Society, 2011, pp. 643–650.
- [47] G. Cheng, J. Yang, D. Gao, L. Guo, and J. Han, "High-quality proposals for weakly supervised object detection," *IEEE Trans. Image Process.*, vol. 29, pp. 5794–5804, 2020.
- [48] H. Bilen, M. Pedersoli, and T. Tuytelaars, "Weakly supervised object detection with convex clustering," in *CVPR*. IEEE Computer Society, 2015, pp. 1081–1089.
- [49] T. Lin, X. Zhao, and Z. Shou, "Single shot temporal action detection," in *ACM Multimedia*. ACM, 2017, pp. 988–996.
- [50] L. Yang, H. Peng, D. Zhang, J. Fu, and J. Han, "Revisiting anchor mechanisms for temporal action localization," *IEEE Trans. Image Process.*, vol. 29, pp. 8535–8548, 2020.
- [51] Y. Zhao, Y. Xiong, L. Wang, Z. Wu, X. Tang, and D. Lin, "Temporal action detection with structured segment networks," in *ICCV*. IEEE Computer Society, 2017, pp. 2933–2942.
- [52] J. Li, B. Zhang, Y. Wang, Y. Tai, Z. Zhang, C. Wang, J. Li, X. Huang, and Y. Xia, "ASFD: automatic and scalable face detector," in *ACM Multimedia*. ACM, 2021, pp. 2139–2147.
- [53] L. Wang, Y. Xiong, D. Lin, and L. V. Gool, "Untrimmednets for weakly supervised action recognition and detection," in *CVPR*. IEEE Computer Society, 2017, pp. 6402–6411.
- [54] P. Nguyen, T. Liu, G. Prasad, and B. Han, "Weakly supervised action localization by sparse temporal pooling network," in *CVPR*. Computer Vision Foundation / IEEE Computer Society, 2018, pp. 6752–6761.
- [55] P. X. Nguyen, D. Ramanan, and C. C. Fowlkes, "Weakly-supervised action localization with background modeling," in *ICCV*. IEEE, 2019, pp. 5501–5510.
- [56] H. Su, X. Zhao, and T. Lin, "Cascaded pyramid mining network for weakly supervised temporal action localization," in *ACCV (2)*, ser. Lecture Notes in Computer Science, vol. 11362. Springer, 2018, pp. 558–574.
- [57] P. Lee and H. Byun, "Learning action completeness from points for weakly-supervised temporal action localization," in *ICCV*. IEEE, 2021, pp. 13628–13637.
- [58] C. Ju, P. Zhao, Y. Zhang, Y. Wang, and Q. Tian, "Point-level temporal action localization: Bridging fully-supervised proposals to weakly-supervised losses," *CoRR*, vol. abs/2012.08236, 2020.
- [59] C. Ju, P. Zhao, S. Chen, Y. Zhang, Y. Wang, and Q. Tian, "Divide and conquer for single-frame temporal action localization," in *ICCV*. IEEE, 2021, pp. 13435–13444.
- [60] F. Ma, L. Zhu, Y. Yang, S. Zha, G. Kundu, M. Feiszli, and Z. Shou, "Sf-net: Single-frame supervision for temporal action localization," in *ECCV (4)*, ser. Lecture Notes in Computer Science, vol. 12349. Springer, 2020, pp. 420–437.
- [61] S. Narayan, H. Cholakkal, F. S. Khan, and L. Shao, "3c-net: Category count and center loss for weakly-supervised action localization," in *ICCV*. IEEE, 2019, pp. 8678–8686.
- [62] A. Vaswani, N. Shazeer, N. Parmar, J. Uszkoreit, L. Jones, A. N. Gomez, L. Kaiser, and I. Polosukhin, "Attention is all you need," in *NIPS*, 2017, pp. 5998–6008.
- [63] B. Shi, Q. Dai, Y. Mu, and J. Wang, "Weakly-supervised action localization by generative attention modeling," in *CVPR*. Computer Vision Foundation / IEEE, 2020, pp. 1006–1016.
- [64] D. P. Kingma and M. Welling, "Auto-encoding variational bayes," in *ICLR*, 2014.
- [65] A. Pardo, H. Alwassel, F. C. Heilbron, A. K. Thabet, and B. Ghanem, "RefineLoc: Iterative refinement for weakly-supervised action localization," in *WACV*. IEEE, 2021, pp. 3318–3327.
- [66] Z. Luo, D. Guillory, B. Shi, W. Ke, F. Wan, T. Darrell, and H. Xu, "Weakly-supervised action localization with expectation-maximization multi-instance learning," in *ECCV (29)*, vol. 12374. Springer, 2020, pp. 729–745.
- [67] D. Moltisanti, S. Fidler, and D. Damen, "Action recognition from single timestamp supervision in untrimmed videos," in *CVPR*. Computer Vision Foundation / IEEE, 2019, pp. 9915–9924.
- [68] H. Idrees, A. R. Zamir, Y. Jiang, A. Ghorban, I. Laptev, R. Sukthankar, and M. Shah, "The THUMOS challenge on action recognition for videos 'in the wild'," *Comput. Vis. Image Underst.*, vol. 155, pp. 1–23, 2017.
- [69] F. C. Heilbron, V. Escorcia, B. Ghanem, and J. C. Niebles, "Activitynet: A large-scale video benchmark for human activity understanding," in *CVPR*. IEEE Computer Society, 2015, pp. 961–970.
- [70] A. Wedel, T. Pock, C. Zach, H. Bischof, and D. Cremers, "An improved algorithm for tv-L¹ optical flow," in *Statistical and Geometrical Approaches to Visual Motion Analysis*, ser. Lecture Notes in Computer Science. Springer, 2008, vol. 5604, pp. 23–45.
- [71] Z. Shou, H. Gao, L. Zhang, K. Miyazawa, and S. Chang, "Autoloc: Weakly-supervised temporal action localization in untrimmed videos," in *ECCV (16)*, ser. Lecture Notes in Computer Science, vol. 11220. Springer, 2018, pp. 162–179.
- [72] J. Feng, F. Hong, and W. Zheng, "MIST: multiple instance self-training framework for video anomaly detection," in *CVPR*. Computer Vision Foundation / IEEE, 2021, pp. 14009–14018.
- [73] J. Lei, L. Li, L. Zhou, Z. Gan, T. L. Berg, M. Bansal, and J. Liu, "Less is more: Clipbert for video-and-language learning via sparse sampling," in *CVPR*. Computer Vision Foundation / IEEE, 2021, pp. 7331–7341.
- [74] J. Hu, L. Shen, and G. Sun, "Squeeze-and-excitation networks," in *CVPR*. Computer Vision Foundation / IEEE Computer Society, 2018, pp. 7132–7141.
- [75] B. Xu, Y. Fu, Y. Jiang, B. Li, and L. Sigal, "Heterogeneous knowledge transfer in video emotion recognition, attribution and summarization," *IEEE Trans. Affect. Comput.*, vol. 9, no. 2, pp. 255–270, 2018.
- [76] A. Neubeck and L. V. Gool, "Efficient non-maximum suppression," in *ICPR (3)*. IEEE Computer Society, 2006, pp. 850–855.
- [77] J. See, M. H. Yap, J. Li, X. Hong, and S. Wang, "MEGC 2019 - the second facial micro-expressions grand challenge," in *FG*. IEEE, 2019, pp. 1–5.
- [78] D. P. Kingma and J. Ba, "Adam: A method for stochastic optimization," in *ICLR (Poster)*, 2015.
- [79] Y. He, S. Wang, J. Li, and M. H. Yap, "Spotting macro-and micro-expression intervals in long video sequences," in *FG*. IEEE, 2020, pp. 742–748.
- [80] L. Zhang, J. Li, S. Wang, X. Duan, W. Yan, H. Xie, and S. Huang, "Spatio-temporal fusion for macro- and micro-expression spotting in long video sequences," in *FG*. IEEE, 2020, pp. 734–741.
- [81] Y. He, "Research on micro-expression spotting method based on optical flow features," in *ACM Multimedia*. ACM, 2021, pp. 4803–4807.

- [82] G. B. Liong, S. Liong, J. See, and C. Chee-Seng, "MTSN: A multi-temporal stream network for spotting facial macro-and micro-expression with hard and soft pseudo-labels," in *Proceedings of the 2nd Workshop on Facial Micro-Expression: Advanced Techniques for Multi-Modal Facial Expression Analysis*, 2022, pp. 3–10.
- [83] Y. Zhao, X. Tong, Z. Zhu, J. Sheng, L. Dai, L. Xu, X. Xia, Y. Jiang, and J. Li, "Rethinking optical flow methods for micro-expression spotting," in *ACM Multimedia*. ACM, 2022, pp. 7175–7179.



Wang-Wang Yu received the M.S. degree in biomedical engineering from University of Electronic Science and Technology of China (UESTC) in 2020. He is now pursuing his Ph.D. degree in UESTC. His research interests include video understanding, emotional analysis, weakly-supervised learning.



Kai-Fu Yang received the Ph.D. degree in biomedical engineering from the University of Electronic Science and Technology of China (UESTC), Chengdu, China, in 2016. He is currently an associate research professor with the MOE Key Lab for Neuroinformation, School of Life Science and Technology, UESTC, Chengdu, China. His research interests include cognitive computing and brain-inspired computer vision.



Hong-Mei Yan received the Ph.D. degree in biomedical engineering from Chongqing University in 2003. She is now a Professor with the MOE Key Laboratory for Neuroinformation, University of Electronic Science and Technology of China, Chengdu, China. Her research interests include visual cognition, visual attention, visual encoding and decoding.



Yong-Jie Li (Senior Member, IEEE) received the Ph.D. degree in biomedical engineering from UESTC, in 2004. He is currently a Professor with the Key Laboratory for NeuroInformation of Ministry of Education, School of Life Science and Technology, University of Electronic Science and Technology of China. His research focuses on building of biologically inspired computational models of visual perception and the applications in image processing and computer vision.